Brief Communication

Kidney360

Loss of Cilia Does Not Slow Liver Disease Progression in Mouse Models of Autosomal Recessive Polycystic Kidney Disease

Anna Rachel Gallagher[1] *and Stefan Somlo*[1,2]

KIDNEY360 1: 962–968, 2020. doi: https://doi.org/10.34067/KID.0001022019

Introduction

Autosomal dominant polycystic kidney disease (ADPKD) is a hereditary disorder characterized by abnormal cellular proliferation, cyst fluid accumulation, extracellular matrix remodeling, and fibrosis in the kidney and liver. ADPKD accounts for approximately 5% of the prevalent adult RRT (dialysis or transplantation) population, with most cases resulting from mutations in *PKD1* or *PKD2*, which encodes polycystin-1 (PC1) or polycystin-2 (PC2), respectively (1). In contrast, autosomal recessive polycystic kidney disease (ARPKD) is a rare and severe form of polycystic disease affecting the kidneys and biliary tract of children with an estimated incidence of 1 in 20,000 live births (2). ARPKD develops *in utero* and is diagnosed early in life, often prenatally. The clinical spectrum is widely variable, with approximately 20% of cases severely affected at birth, whereas the remainder are affected more as juveniles. Clinical findings in ARPKD include enlarged echogenic kidneys due to fusiform dilation of the collecting ducts and dilated bile ducts accompanied by congenital hepatic fibrosis resulting in portal hypertension (2). Mutations in *PKHD1* are responsible for most typical cases of ARPKD (3,4). It encodes a heavily glycosylated approximately 450-kD single-pass transmembrane protein, fibrocystin (FPC), that localizes to the primary cilia, basal bodies, apical membrane, and exosome-like vesicles in kidney and liver epithelial cells (5–7). The function of FPC is largely unknown, but it has been proposed to act as a ligand or cell surface coreceptor that undergoes Notch-like processing and plays a role in regulating mitotic spindle orientation (8–10).

Several rodent models for ARPKD have been reported with all but one targeting the 5′ region of the *Pkhd1* gene. These models invariably exhibit biliary cysts accompanied by periportal fibrosis consistent with the human disease (5,11,12). The renal phenotype is mild in the rat model and largely absent from the mouse models. Recently, $Pkhd1^{del67}$, a mouse model generated by lacking the last 137 amino acids of the intracellular domain, had no discernible kidney or liver phenotype, suggesting that the region of FPC required for normal function *in vivo* resides in the extracellular and transmembrane domains (13). A functional interaction between ARPKD and ADPKD has been described whereby reduced dosage of *Pkd1* worsens the ARPKD phenotype in mice (11,14). Cilia structure and function have been strongly associated with fibrocystic genetic disorders collectively termed ciliopathies. Models lacking cilia or having alterations in the protein composition in cilia recapitulate fibrocystic kidney and liver phenotypes, supporting the hypothesis that kidney and bile duct cyst formation results from aberrant ciliary function (15). Inactivation of PC1 or PC2, which is expressed on primary cilia, gives rise to ADPKD; however, concomitant removal of cilia at the time of *Pkd1* or *Pkd2* inactivation markedly reduces cyst growth *in vivo* (16). These data show that ADPKD occurs when intact cilia devoid of polycystins support an unchecked activity that fosters cystic tissue remodeling by a cilia-dependent cyst-activating (CDCA) signal.

Because the intact primary cilium is central to the pathogenesis of ADPKD and a genetic interaction between ADPKD and ARPKD exists, we sought to determine whether intact cilia affect the phenotypic expression of ARPKD. Here, we report that conditional inactivation of cilia in mice with germline inactivation of *Pkhd1* does not affect the *in vivo* phenotype. When *Pkhd1* inactivation is combined with haploinsufficiency for *Pkd1*, the increased severity normally caused by this combination is ameliorated by inactivation of cilia, confirming the cilia dependence of the additive effect of *Pkd1* dosage reduction in ARPKD. Our data show that unlike ADPKD, cyst formation due to loss of germline *Pkhd1* in ARPKD is not slowed by the absence of intact cilia.

Materials and Methods

Mouse Strains and Histology

The mouse strains used in this study have previously been described: $Pkhd1^{del4}$ (5), $Kif3a^{flox}$ (16), UBC-cre^{ER} (16), and $Pkd1^{+/-}$ (14). These animals are predominantly on a C57BL/6 genetic background. UBC-cre^{ER} mice were induced with tamoxifen (T5648; Sigma) delivered by intraperitoneal injection at a dose of

[1]Department of Internal Medicine (Nephrology), Yale School of Medicine, New Haven, Connecticut
[2]Department of Genetics, Yale School of Medicine, New Haven, Connecticut

Correspondence: Anna Rachel Gallagher or Stefan Somlo, Section of Nephrology, Yale School of Medicine, PO Box 208029, 333 Cedar Street, New Haven, CT 06520. Email: anna-rachel.gallagher@yale.edu or stefan.somlo@yale.edu

2 mg daily from postnatal day 28 to 32. Mice were analyzed at 17 weeks of age. At the end of the treatment, mice were perfusion fixed with 4% paraformaldehyde, liver tissue was harvested, and some tissue was embedded in paraffin for histochemical analysis. Liver sections were processed and stained with hematoxylin and eosin or other specific markers. The allocation of animals to experimental and control groups was solely on the basis of genotype, irrespective of sex and without any exclusions. All animals were used in accordance with scientific, humane, and ethical principles and in compliance with regulations approved by the Yale University Institutional Animal Care and Use Committee.

Immunohistochemistry

For cytokeratin-19 (CK19; 1:100, TROMA III; DSHB Iowa) immunostaining, sections were deparaffinized in xylene (3×10 minutes) and hydrated in ethanol (3×10 minutes) followed by blocking in methanol:hydrogen peroxide (10%) for 30 minutes at room temperature. EDTA antigen retrieval was used to unmask the antigen recognized by the TROMA-III antibody, and then, the samples were rinsed in 0.05% Tween 20 in PBS (3×5 minutes; 1× PBS, pH 7.4), blocked with 1% BSA prior to adding the primary antibody, and incubated overnight at 4°C. The liver sections were rinsed with 0.05% Tween 20 in 1× PBS (3×5 minutes), incubated for 30 minutes at room temperature with secondary antibody (A10549; goat anti-rat horseradish peroxidase; 1:500; Invitrogen), and finally, developed with 3–3′-diaminobenzidine according to the manufacturer's instructions (Sk-4100; Vector Labs). The sections were counterstained with Harris hematoxylin (1:10, GH5380; Sigma) for 10 seconds, washed in distilled water (10 minutes), and dehydrated (ethanol [3×5 minutes] and xylene [3×5 minutes]) before being mounted using sub-X clearing media (3801741; Leica Microsystems Inc.). Immunofluorescence staining for cilia was performed on liver cryosections using Arl13B (1:200, 17711–1-AP; Proteintech) as a ciliary marker and E-cadherin (1:200, 610182; R&D transduction) to label the biliary epithelia. The immunolabeling protocol was carried out as previously described (16). The images were obtained on a Nikon TE2000U microscope (Nikon, Bloomfield, CT).

Morphometric Quantification of CK19-Positive Structures and Cystic Index

Slides labeled with CK19 underwent computer-assisted morphometric analysis using a motorized stage system to scan the large liver lobe at 4× magnification and the Metamorph software (Molecular Devices, Downington, PA). Data were expressed as the percentage of the whole-liver lobe area occupied by CK19-positive cells. The setup consisted of a Nikon Eclipse TE2000U microscope, a motorized stage system (Rockland, MA), and a photometric cool snap HQ digital camera (Roper Scientific, Tucson, AZ). Biliary cyst analysis for the CK19 population and hepatic cystic index were calculated as described (17). Data were expressed as the percentage of the whole-liver lobe area.

Oil Red O Staining

Oil Red O working solution (O0625–25G; Sigma) was prepared with 60% isopropanol to make a 0.5% stock solution. The stock solution was diluted with double-distilled water at a 3:2 ratio (3 ml of stock solution and 2 ml of double-distilled water), filtered, and allowed to stand for at least 10 minutes at room temperature; 8-μm cryosections of fixed liver tissue were cut and placed at room temperature for 30 minutes. The slides were rinsed with 60% isopropanol, then stained with freshly prepared Oil Red O working solution for 15 minutes, and rinsed in 60% isopropanol. The nuclei were stained with 10% Harris hematoxylin for 10 seconds and then rinsed with distilled water. The slides were mounted with Mowiol mounting medium and analyzed.

Sample Size and Power Calculation

Sample size and power calculations were performed using STPLAN (version 4.5; University of Texas, MD Anderson Cancer Center). Calculations were on the basis of the following: the mean liver-body weight ratio in *Pkhd1*$^{del4/del4}$ livers at 17 weeks is 6.15% (SD of ±0.72) on the basis of empirical data. Our alternative hypothesis was that loss of cilia in *Pkhd1*$^{del4/del4}$ livers and cilia double-mutant livers would result in a 20% decrease in liver-body weight ratio to 4.9% with a significance level (α) of 0.05 (two sided). Under these expectations, seven mice could achieve 80% power and ten mice could achieve 95% power to detect the difference of 1.25 liver-body weight ratio between the null hypothesis and the alternative hypothesis. Data were analyzed by one-way ANOVA followed by Tukey' multiple-comparison test with GraphPad Prism 8.4.1 software. The Brown–Forsythe test or Bartlett test was used to test for the equality of group variances. $P=0.05$ was considered significant. All data are presented as mean±SD.

Results

Because cilia transmit a cyst-promoting signal that is activated upon removal of *Pkd1* or *Pkd2*, we investigated whether a similar cilia-dependent signaling mechanism modulates *Pkhd1* liver cyst progression in an orthologous model of ARPKD. The *Pkhd1*$^{del4/del4}$ mouse model develops biliary cysts accompanied by periportal fibrosis (8). It has no discernible kidney phenotype. To inactivate cilia in this model, we used a tamoxifen-inducible *UBC-cre*^{ER} that has a general promoter (ubiquitin-C) active in many tissues, including bile duct–derived epithelia (16). To draw direct comparison with previous studies inactivating cilia in ADPKD models, we used the *Kif3a* floxed allele for inducible cilia inactivation (16). Mice were induced with tamoxifen from postnatal day 28 to 32 to activate cre recombinase and examined 13 weeks after the start of induction at age 17 weeks (Figure 1A). The extent of liver disease in the *Pkhd1*$^{del4/del4}$ animals at the time of tamoxifen administration to initiate cilia inactivation was mild, with some bile duct expansion reminiscent of von Meyenburg complexes (Figure 1B). At 17 weeks, the *Pkhd1*$^{del4/del4}$ animals developed more cystic bile ducts with increased liver-body weight ratio and biliary structures as denoted by areas of CK19-positive staining and increased hepatic cystic area compared with littermate controls (Figure 1, C and D). Cilia knockout double-mutant mice, *UBC-cre*^{ER}; *Kif3a*$^{fl/fl}$; *Pkhd1*$^{del4/del4}$, developed biliary cysts with quantitative hepatic parameters indistinguishable from *Pkhd1*$^{del4/del4}$ alone

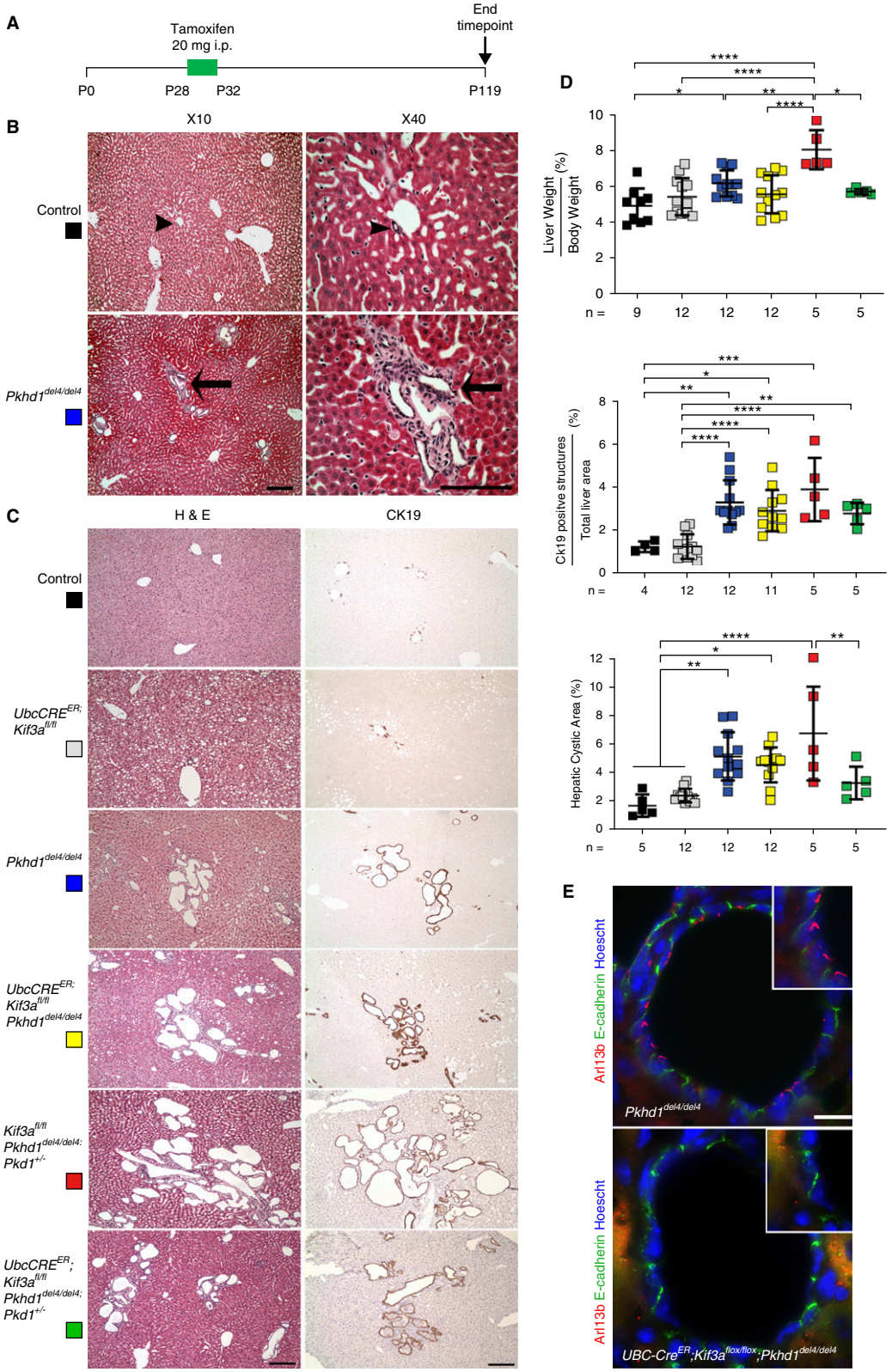

Figure 1. | **Inactivation of cilia does not affect cyst progression in *Pkhd1*$^{del4/del4}$ livers.** (A) Schematic diagram of the course of tamoxifen induction for cilia inactivation and study end point. i.p., intraperitoneal. (B) Histologic representation of littermate control (arrowheads) and *Pkhd1*$^{del4/del4}$ (arrows) bile ducts at postnatal day 28 (P28) prior to inactivation of cilia. *Pkhd1*$^{del4/del4}$ livers exhibit mild bile duct proliferation accompanied by von Meyenburg complexes indicated by arrows. Scale bars, 500 μm in 10× panel; 40 μm in 40× panel. (C) Representative hematoxylin and eosin (H&E)– and cytokeratin-19 (CK19)–stained sections show biliary epithelia of the indicated allelic combinations induced

with tamoxifen from P28-^{32}P and examined at 17 weeks of age. Single *Kif3a* knockouts (*UBC-cre^{ER}; Kif3a $^{fl/fl}$*; gray squares) show mild bile duct proliferation as previously described (16). *Pkhd1$^{del4/del4}$* animals have extensive bile duct cyst formation (blue squares), and double knockouts of *Pkhd1* and *Kif3a* (*UBC-cre^{ER}; Kif3a $^{fl/fl}$; Pkhd1$^{del4/del4}$*; yellow squares) showed no significant difference in cystic disease progression compared with *Pkhd1$^{del4/del4}$* alone. Representative images of livers from *Kif3a$^{fl/fl}$; Pkhd1$^{del4/del4}$; Pkd1$^{+/-}$* (red squares) show enhanced cystic disease progression due to reduced *Pkd1* dosage. This incremental worsening is improved upon removal of cilia in *UBC-cre^{ER}; Kif3a $^{fl/fl}$; Pkhd1$^{del4/del4}$; Pkd1$^{+/-}$* (green squares). Scale bar, 500 μM. (D) Quantitation of differences in liver phenotypes at 17 weeks for the allele combinations in (C). The color squares correspond to the genotypes in (C). *Pkhd1$^{del4/del4}$* (blue squares) shows significant increase in liver weight-body weight ratio, CK19-positive population, and hepatic cystic area compared with littermate controls (black squares). Significant increase in CK19 population and hepatic cystic area was observed in *Pkhd1$^{del4/del4}$* livers compared with *Ubc-cre^{ER}; Kif3a$^{fl/fl}$* livers (gray squares), but there was no difference with *UBC-cre^{ER}; Kif3a$^{fl/fl}$; Pkhd1$^{del4/del4}$* (yellow squares) cilia and *Pkhd1* double-knockout livers. *Kif3a$^{fl/fl}$; Pkhd1$^{del4/del4}$; Pkd1$^{+/-}$* (red squares) mice with reduced *Pkd1* dosage have significantly increased liver weight/body weight relative to all other groups, and inactivation of cilia in these mice (*UBC-cre^{ER}; Kif3a $^{fl/fl}$; Pkhd1$^{del4/del4}$; Pkd1$^{+/-}$*; green squares) counteracts the effect of *Pkd1* haploinsufficiency as indicated by significantly improved liver weight-body weight ratio and hepatic cystic area. Each square represents a single animal; both males and females were used. The absolute number of animals used for each genotype is displayed under the graph. Multiple group comparisons were performed using one-way ANOVA followed by Tukey multiple comparison test and are presented as the mean±SD. *P=0.05; **P=0.01; ***P<0.001; ****P<0.001. (E) Immunohistochemistry for Arl13b (red) and E-cadherin (green) in bile duct cysts from mice with loss of *Pkhd1* alone or in combination with conditional inactivation of *Kif3a* at 17 weeks of age. Cilia were present in the cyst lining epithelia of the *Pkhd1$^{del4/del4}$* mutant but absent from the *UBC-cre^{ER}; Kif3a$^{fl/fl}$; Pkhd1$^{del4/del4}$* cells. The nuclei are marked by Hoechst stain in blue. Scale bar, 100 μM.

(Figure 1, C and D). Immunohistochemical analysis of cystic epithelia with Arl13b antisera shows the presence of cilia in the *Pkhd1$^{del4/del4}$* cyst lining epithelia, whereas the *UBC-cre^{ER}; Kif3a$^{fl/fl}$; Pkhd1$^{del4/del4}$* cystic epithelia were devoid of cilia (Figure 1E). Removing cilia postnatally does not have a significant effect on the liver cystic disease progression due to loss of *Pkhd1*.

Previous work describes a genetic interaction between *Pkhd1* and *Pkd1*, with reduced *Pkd1* levels worsening the cystic phenotype in ARPKD models in both the kidney and liver (5,11). In order to address whether loss of cilia can ameliorate the cyst-promoting effect of reduced *Pkd1* dosage on a *Pkhd1* loss of function background, we generated mice with the following allelic combinations: *Kif3a$^{fl/fl}$; Pkhd1$^{del4/del4}$; Pkd1$^{+/-}$* and *UBC-cre^{ER}; Kif3a$^{fl/fl}$; Pkhd1$^{del4/del4}$; Pkd1$^{+/-}$*. All animals were treated with tamoxifen following the same induction regimen (Figure 1A). Loss of one copy of *Pkd1* in *Pkhd1*-deficient bile ducts significantly increased the liver weight-body weight ratio compared with the *Pkhd1$^{del4/del4}$* alone (Figure 1, C and D). Inactivating *Kif3a* (cilia) on this background significantly improved the presumed *Pkd1*-dependent component of cystic growth when comparing the liver weight-body weight ratio and hepatic cystic area, returning these parameters to the baseline *Pkhd1$^{del4/del4}$* phenotype (Figure 1, C and D). The data show that the incremental cyst-promoting effect of germline heterozygous loss of *Pkd1* on a *Pkhd1*-deficient background can be eliminated by the inactivation of cilia at a postdevelopmental time point early in the course of bile duct cyst growth. The *Pkd1* dosage-dependent component of enhanced cyst formation in models of ARPKD is dependent on the continued presence of intact cilia, much like CDCA in ADPKD.

Loss of cilia alone (*UBC-cre^{ER}; Kif3a$^{fl/fl}$*) resulted in minimal bile duct proliferation with similar liver phenotype to littermate controls at 17 weeks of age (Figure 1, C and D). Although postnatal inactivation of cilia did not result in significant cystic disease pathology in the liver, the animals lacking Kif3a and cilia did have significantly increased body weight compared with control and *Pkhd1$^{del4/del4}$* animals (Figure 2A). Histologic analysis of liver sections using Oil Red O staining confirmed a marked increase in fat droplets in *UBC-cre^{ER}; Kif3a$^{fl/fl}$* and *UBC-cre^{ER}; Kif3a$^{fl/fl}$; Pkhd1$^{del4/del4}$* livers, indicative of hepatic steatosis due to a loss of cilia, which has been previously described (18) (Figure 2C). Sex differences were only apparent within the *UbcCre; Kif3a$^{fl/fl}$* animals with regard to total liver weight (Figure 2B).

Discussion

The role of cilia in cystic disease is supported by findings that orthologous ADPKD proteins localize to cilia, that genetic ablation of cilia results in cystic disease, and that a cilia-dependent signal is regulated by polycystins (16). The striking feature of the latter finding is that ADPKD cyst growth following loss of polycystins is markedly attenuated if cells also lack cilia. This defines the role of polycystins as regulating a CDCA signal (16). This finding has been further refined by recent studies showing that impaired trafficking of membrane-associated proteins into cilia without other overt changes in cilia structure can similarly antagonize cyst growth resulting from the absence of polycystins (19). In light of these findings, mechanisms to pharmacologically reduce cilia length have been one suggested approach to putative therapy for ADPKD (20).

We sought to address whether similar cilia-targeted strategies would have potential value for ARPKD. In support of such an approach, it is noted that the histopathology of ARPKD bears resemblance to the recessive ciliopathy disorders in which ductal plate malformations resulting in congenital hepatic fibrosis are a common feature (21). Many ciliopathy genes are required for proper structure and protein composition of cilia, and *Pkhd1* has been implicated in ciliogenesis (22). Furthermore, there is a functional interaction between ARPKD and ADPKD (11,14). Reduced dosage of *Pkd1* worsens the ARPKD phenotype in mice. Despite these varied connections, this study shows that removal of cilia does not substantially affect the fibrocystic liver disease progression in *Pkhd1* inactivation. We did find that the relative worsening of the ARPKD phenotype in the setting of reduced dosage of *Pkd1* is dependent on the presence of intact cilia. These data can be interpreted to suggest that the nature of the genetic interaction between *Pkd1* and *Pkhd1* is

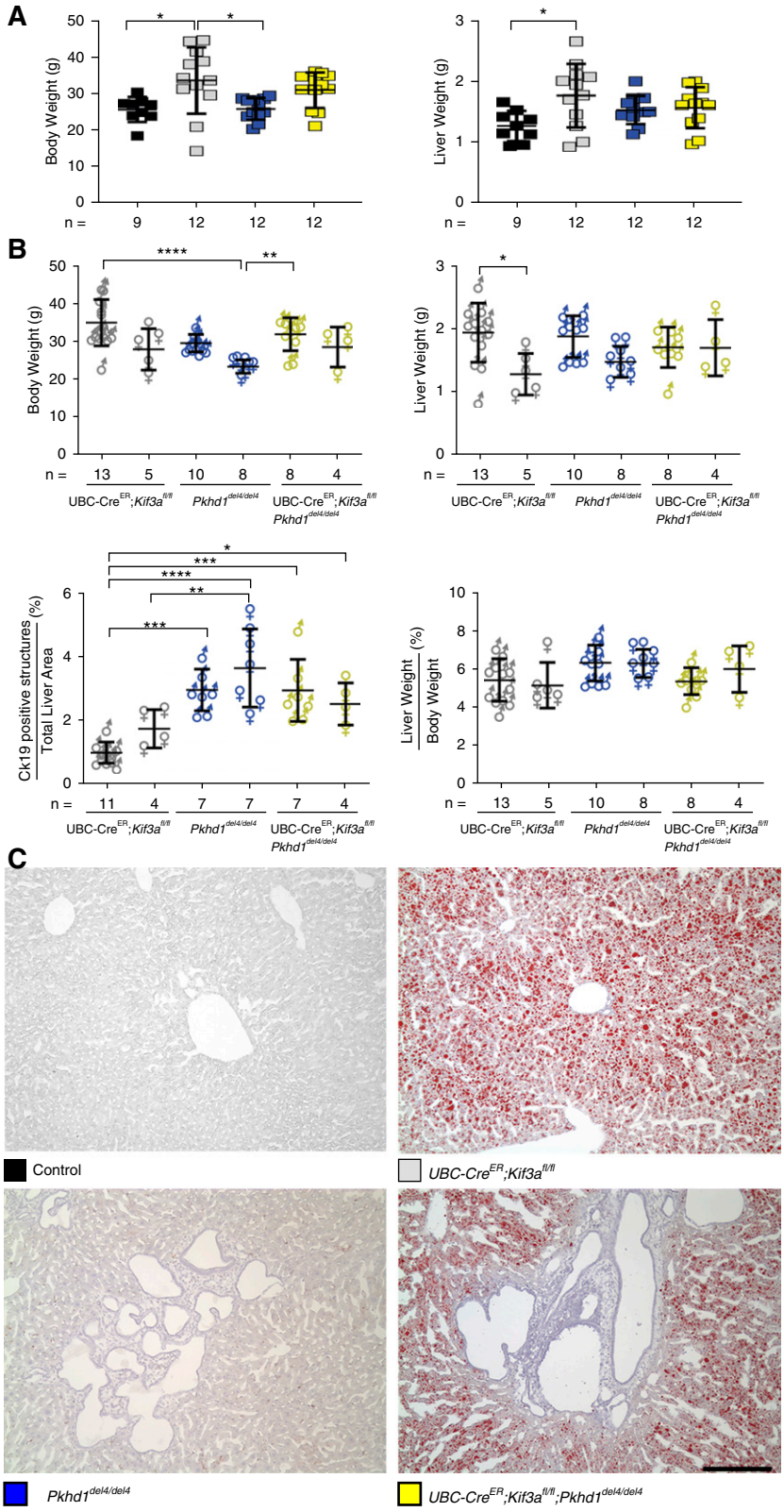

Figure 2. | **Loss of cilia results in increased body weight and hepatic steatosis.** (A) Comparison of body and liver weights of mice with the indicated genotypes. Colored squares show corresponding genotypes in (A and C). Loss of cilia in *Kif3a* single knockouts (gray squares) resulting in a significant increase in body and liver weight compared with controls (black squares). (B) Graphical representation of the physiologic parameters of the different sexes used in this study. Male (♂) and female (♀) data for total body weight, liver weight, liver weight-body weight ratio, and cytokeratin-19 (CK19)–positive structures were analyzed for sex differences. Sex differences were only evident in the Kif3a (*UbcCre;*

Kif3a$^{fl/fl}$) mutant animals when comparing liver weights. Multiple group comparisons were performed using one-way ANOVA followed by Tukey multiple comparison test and are presented as the mean±SD. *P=0.05; **P=0.01; ***P<0.001; ****P<0.001. (C) Hepatic steatosis was evident by the presence of fat droplets as identified by Oil Red O stain in the cilia-deficient mutants. Scale bar, 400 μM.

indirect—that they do not function in a common pathway. It suggests that loss of *Pkhd1* sensitizes cells to CDCA so that even mild increases in CDCA activity resulting from a graded decrease in *Pkd1* dosage by 50% are sufficient to elicit a mildly worsening cyst-promoting effect. The graded CDCA response seems to still be polycystin dependent because removal of cilia reverses this incremental effect without eliminating the underlying disease process due to a mutation in *Pkhd1*.

Finally, the data show that inactivation of cilia at 4 weeks age can still abrogate this *Pkd1* dosage-dependent worsening even though the reduced dosage of PC1 and absence of FPC are transmitted through the germline. This indicates that inhibition of CDCA does not require concomitant inactivation of polycystins and cilia (16) but rather, can occur with delayed inactivation of cilia. This may have implications for therapeutic utility and timing of targeting CDCA in ADPKD. In aggregate, the findings show that the liver disease resulting from loss of *Pkhd1* in ARPKD is not significantly affected by cilia function in the way that it is in ADPKD. This indicates that despite genetic interaction between *Pkhd1* and *Pkd1*, they do not seem to function in a common CDCA-related molecular pathway in bile ducts.

Disclosures

S. Somlo is a founder, shareholder, consultant, and scientific advisory board member for Goldfinch Bio, and has received honoraria from Otsuka Pharmaceuticals. The remaining author has nothing to disclose.

Funding

This work was supported by the Human and Health Services Department, National Institutes of Health, and National Institute of Diabetes and Digestive and Kidney Diseases grant DK100592 (to S. Somlo).

Acknowledgments

We acknowledge the technical assistance of Lonnette Diggs in the Animal Physiology Core at the George M. O'Brien Kidney Center at Yale supported by National Institutes of Health grant P30 DK079310, outside the submitted work.

S. Somlo reports personal fees and other from Goldfinch Bio, and reports personal fees from Otsuka Pharma, outside the submitted work.

Author Contributions

A. Gallagher was responsible for investigation, carried out all of the experimental work, and wrote the manuscript; and S. Somlo reviewed and edited the manuscript.

References

1. Torres VE, Harris PC: Polycystic kidney disease: Genes, proteins, animal models, disease mechanisms and therapeutic opportunities. *J Intern Med* 261: 17–31, 2007
2. Guay-Woodford LM, Desmond RA: Autosomal recessive polycystic kidney disease: The clinical experience in North America. *Pediatrics* 111: 1072–1080, 2003
3. Onuchic LF, Furu L, Nagasawa Y, Hou X, Eggermann T, Ren Z, Bergmann C, Senderek J, Esquivel E, Zeltner R, Rudnik-Schöneborn S, Mrug M, Sweeney W, Avner ED, Zerres K, Guay-Woodford LM, Somlo S, Germino GG: PKHD1, the polycystic kidney and hepatic disease 1 gene, encodes a novel large protein containing multiple immunoglobulin-like plexin-transcription-factor domains and parallel beta-helix 1 repeats. *Am J Hum Genet* 70: 1305–1317, 2002
4. Ward CJ, Hogan MC, Rossetti S, Walker D, Sneddon T, Wang X, Kubly V, Cunningham JM, Bacallao R, Ishibashi M, Milliner DS, Torres VE, Harris PC: The gene mutated in autosomal recessive polycystic kidney disease encodes a large, receptor-like protein. *Nat Genet* 30: 259–269, 2002
5. Gallagher AR, Esquivel EL, Briere TS, Tian X, Mitobe M, Menezes LF, Markowitz GS, Jain D, Onuchic LF, Somlo S: Biliary and pancreatic dysgenesis in mice harboring a mutation in Pkhd1. *Am J Pathol* 172: 417–429, 2008
6. Hogan MC, Manganelli L, Woollard JR, Masyuk AI, Masyuk TV, Tammachote R, Huang BQ, Leontovich AA, Beito TG, Madden BJ, Charlesworth MC, Torres VE, LaRusso NF, Harris PC, Ward CJ: Characterization of PKD protein-positive exosome-like vesicles. *J Am Soc Nephrol* 20: 278–288, 2009
7. Ward CJ, Yuan D, Masyuk TV, Wang X, Punyashthiti R, Whelan S, Bacallao R, Torra R, LaRusso NF, Torres VE, Harris PC: Cellular and subcellular localization of the ARPKD protein; fibrocystin is expressed on primary cilia. *Hum Mol Genet* 12: 2703–2710, 2003
8. Hiesberger T, Gourley E, Erickson A, Koulen P, Ward CJ, Masyuk TV, Larusso NF, Harris PC, Igarashi P: Proteolytic cleavage and nuclear translocation of fibrocystin is regulated by intracellular Ca2+ and activation of protein kinase C. *J Biol Chem* 281: 34357–34364, 2006
9. Kaimori JY, Nagasawa Y, Menezes LF, Garcia-Gonzalez MA, Deng J, Imai E, Onuchic LF, Guay-Woodford LM, Germino GG: Polyductin undergoes notch-like processing and regulated release from primary cilia. *Hum Mol Genet* 16: 942–956, 2007
10. Nishio S, Tian X, Gallagher AR, Yu Z, Patel V, Igarashi P, Somlo S: Loss of oriented cell division does not initiate cyst formation. *J Am Soc Nephrol* 21: 295–302, 2010
11. Garcia-Gonzalez MA, Menezes LF, Piontek KB, Kaimori J, Huso DL, Watnick T, Onuchic LF, Guay-Woodford LM, Germino GG: Genetic interaction studies link autosomal dominant and recessive polycystic kidney disease in a common pathway. *Hum Mol Genet* 16: 1940–1950, 2007
12. Woollard JR, Punyashtiti R, Richardson S, Masyuk TV, Whelan S, Huang BQ, Lager DJ, vanDeursen J, Torres VE, Gattone VH, LaRusso NF, Harris PC, Ward CJ: A mouse model of autosomal recessive polycystic kidney disease with biliary duct and proximal tubule dilatation. *Kidney Int* 72: 328–336, 2007
13. Outeda P, Menezes L, Hartung EA, Bridges S, Zhou F, Zhu X, Xu H, Huang Q, Yao Q, Qian F, Germino GG, Watnick T: A novel model of autosomal recessive polycystic kidney questions the role of the fibrocystin C-terminus in disease mechanism. *Kidney Int* 92: 1130–1144, 2017
14. Fedeles SV, Tian X, Gallagher AR, Mitobe M, Nishio S, Lee SH, Cai Y, Geng L, Crews CM, Somlo S: A genetic interaction network of five genes for human polycystic kidney and liver diseases defines polycystin-1 as the central determinant of cyst formation. *Nat Genet* 43: 639–647, 2011
15. Lehman JM, Michaud EJ, Schoeb TR, Aydin-Son Y, Miller M, Yoder BK: The Oak ridge polycystic kidney mouse: Modeling ciliopathies of mice and men. *Dev Dyn* 237: 1960–1971, 2008
16. Ma M, Tian X, Igarashi P, Pazour GJ, Somlo S: Loss of cilia suppresses cyst growth in genetic models of autosomal dominant polycystic kidney disease. *Nat Genet* 45: 1004–1012, 2013
17. Spirli C, Okolicsanyi S, Fiorotto R, Fabris L, Cadamuro M, Lecchi S, Tian X, Somlo S, Strazzabosco M: ERK1/2-dependent vascular endothelial growth factor signaling sustains cyst growth in

polycystin-2 defective mice. *Gastroenterology* 138: 360–371.e7, 2010
18. Jacobs DT, Silva LM, Allard BA, Schonfeld MP, Chatterjee A, Talbott GC, Beier DR, Tran PV: Dysfunction of intraflagellar transport-A causes hyperphagia-induced obesity and metabolic syndrome. *Dis Model Mech* 9: 789–798, 2016
19. Legue E, Liem KF Jr.: Tulp3 is a ciliary trafficking gene that regulates polycystic kidney disease. *Curr Biol* 29: 803–812.e5, 2019
20. Nikonova AS, Deneka AY, Kiseleva AA, Korobeynikov V, Gaponova A, Serebriiskii IG, Kopp MC, Hensley HH, Seeger-Nukpezah TN, Somlo S, Proia DA, Golemis EA: Ganetespib limits ciliation and cystogenesis in autosomal-dominant polycystic kidney disease (ADPKD). *FASEB J* 32: 2735–2746, 2018
21. Gunay-Aygun M: Liver and kidney disease in ciliopathies. *Am J Med Genet C Semin Med Genet* 151C: 296–306, 2009
22. Masyuk TV, Huang BQ, Ward CJ, Masyuk AI, Yuan D, Splinter PL, Punyashthiti R, Ritman EL, Torres VE, Harris PC, LaRusso NF: Defects in cholangiocyte fibrocystin expression and ciliary structure in the PCK rat. *Gastroenterology* 125: 1303–1310, 2003

Received: December 16, 2019 **Accepted:** July 9, 2020